JOURNAL OF SPACECRAFT AND ROCKETS
Vol. 37, No. 5, September–October 2000

Fast Drag Prediction Method Using Euler Equations

E. Oktay* and C. O. Asma†
ROKETSAN, Missiles Industries, Inc., Elmadağ, 06780 Ankara, Turkey

A technique to predict the aerodynamic drag from an Euler flow solution is discussed. The method is based on integration of pressure and skin friction on the surface of the body. For the skin-friction calculation, the van Driest skin-friction model is used. Empirical base drag is also included to the drag calculations. Flow solutions are obtained by an unstructured three-dimensional Euler solver. Supersonic attached flows are the focus, rather than subsonic and transonic flows. The method cannot be applied to separated and vortical flows at a high angle of attack. Present calculation technique is applied to three-dimensional supersonic flows around missile geometries. The technique is applied to three different test cases for validation. The first test case is a conventional missile geometry having a fineness ratio of 10 and rectangular fins. The second test case is another conventional missile geometry having a fineness ratio of 16 and sweptback fins. The third test case is a missile geometry with a fineness ratio of 13.06 and having cross-oriented sweptback tail fins and boattail afterbody. Drag coefficients predicted by the present technique are compared with the experimental results obtained at different Mach numbers and angles of attack.

Nomenclature

C_D	=	drag coefficient, $2D/\rho_\infty V_\infty^2 S_{\text{ref}}$
C_f	=	local skin-friction coefficient
C_p	=	pressure coefficient
c	=	chord length, m
D	=	drag force, N
d	=	diameter, m
e	=	total energy per unit volume, J/m^3
$\boldsymbol{F}$	=	flux vector
$\boldsymbol{f}$	=	aerodynamic force vector, N
L	=	axial missile length, m
l	=	characteristic length, m
M	=	Mach number
$\boldsymbol{n}$	=	surface normal unit vector
Pr	=	Prandtl number
p	=	pressure, Pa
$\boldsymbol{Q}$	=	vector of conservative variables
Re	=	Reynolds number, $\rho V l/\mu$
r	=	recovery factor
S	=	cross-sectional area, m^2
s	=	Sutherland constant, K
T	=	temperature, K
t	=	thickness of the fin, m
u, v, w	=	velocity components in x, y, and z directions, m/s
$\boldsymbol{V}$	=	velocity vector, m/s
V	=	volume, m^3
x, y, z	=	Cartesian coordinates
α	=	angle of attack, deg
β	=	angle of side slip, deg
γ	=	specific heats ratio
μ	=	viscosity, N · s/m^2
ρ	=	density, kg/m^3
τ	=	shear stress, Pa

Subscripts

BS	=	base
e	=	edge of boundary-layer
FB	=	forebody
FF	=	far field
ref	=	reference
w	=	wall
x, y, z	=	Cartesian components
0	=	stagnation value
∞	=	far field

Received 8 December 1999; revision received 15 March 2000; accepted for publication 20 March 2000.

*Chief Engineer, Engineering Development Department. Member AIAA.
†Engineer, Engineering Development Department.

Introduction

ACCURATE prediction of aerodynamic drag of missiles has attracted the attention of design engineers and aerodynamicists for many years. Improvement in cruise and/or maneuvering performance of missiles due to the drag reduction is still a high priority challenge for missile design. Although wind-tunnel tests and flight tests are unavoidable requirements for obtaining the drag in the final phase of a missile design, fast prediction methods are preferred by designers during the conceptual and preliminary phases.

There are many methods to predict aerodynamic drag, ranging from semiempirical component buildup methods and potential flow solvers to the Euler and Navier–Stokes solvers. One of the popular computer codes, which use a semiempirical component buildup method, is the Missile DATCOM code.[1] In this code, preliminary body plus interference wave drag data are computed by means of transfer rule method. Skin-friction estimation is also included in the calculations. Another computer code, which is commonly used during the preliminary design phase of the missile, is the SHABP code,[2] which is a panel code. In this code, viscous drag calculation is based on the integration of skin friction on each panel. Limitation of semiempirical methods in their applicability to complex missile geometries and the deficiencies of panel methods have forced aerodynamicists to use other methods, that is, full potential Euler and Navier–Stokes solvers, to predict the aerodynamic drag.

In 1988, the AGARD Fluid Dynamics Panel held a technical status review on computational fluid dynamics- (CFD-) based drag prediction and analysis. In this technical review,[3] various drag prediction techniques were discussed. Although one of the main issues of this study was to point out the important role of various CFD techniques in the prediction of drag, it was stated that "accurate and consistent computation of drag through CFD for complex configurations was not practical because of the time, speed and grid resolution limitations." Since then, significant progress in computer technology, numerical techniques, CAD, and mesh generation tools has been made, and in particular during the last decade, Euler solvers have become an important reference tool for drag calculations. Recently, van Dam et al.[4,5] used an Euler method to predict drag at subsonic and transonic speeds. Their method, which decomposes the total drag into induced and wave drags, is based on the application of the momentum theorem to a control surface enclosing the configuration.

In the current work, a method that is based on the integration of the pressure and skin-friction distribution on the surface of the

body is used. For the skin-friction calculation, the van Driest skin-friction model[6,7] is used. Empirical base drag is also included to the drag calculations. The flow solver used in this study is a three-dimensional unstructured Euler solver, USER3D.[8] This solver has been validated against experimental test results for various test cases in previous work.[9–11]

The present calculation technique is applied to three-dimensional flows around missile geometries at supersonic speeds. Three different test cases are used for the validation of the present technique. The first test case is a conventional missile geometry having a fineness ratio of 10 and rectangular fins. The second test case is another conventional missile geometry having a fineness ratio of 16 and sweptback fins. The third test case is a missile geometry with a fineness ratio of 13.06 having cross-oriented sweptback tail fins and a boattail afterbody. Drag coefficients obtained with the present technique are compared to those of experimental results at different Mach numbers and angles of attack.

Drag-Calculation Methodology

In the present method, total drag is divided into three parts; pressure fore drag, base drag, and viscous drag. Pressure fore drag is calculated by integrating the pressure distribution on the body surface, excluding the base of the missile, which is obtained by a three-dimensional unstructured Euler solver. Base drag is obtained from an empirical formula, which will be given later. To find viscous drag, skin friction that is calculated by the van Driest skin-friction model[6,7] is integrated on the surface of the body. For skin-friction calculations, triangular meshes on the body surface that are used for the Euler solutions are assumed to be individual flat plates. Because the effect of viscosity is added on the inviscid solution using the simple flat plate boundary-layer assumption instead of a viscous solution, separated and vorticity dominated flows cannot be handled with this method.

Aerodynamic force acting on the body in a flow can be obtained by integrating the pressure over the closed control volume enclosing the body. To simplify the calculations, the closed control volume can be decomposed of three parts as: forebody, base, and the far field:

$$\boldsymbol{f} = \int_{\mathrm{FB}} p_w \boldsymbol{n}\,\mathrm{d}s + \int_{\mathrm{FF}} p_\infty \boldsymbol{n}\,\mathrm{d}s + \int_{\mathrm{FB}} \tau_w \boldsymbol{t}\,\mathrm{d}s + \int_{\mathrm{BS}} p_w \boldsymbol{n}\,\mathrm{d}s \tag{1}$$

To include the base drag, integration of the pressure over the far field and on the base in Eq. (1) can be replaced by

$$\int_{\mathrm{FF}} p_\infty \boldsymbol{n}\,\mathrm{d}s + \int_{\mathrm{BS}} p_w \boldsymbol{n}\,\mathrm{d}s = -\frac{2}{\gamma M_\infty^2}\frac{S_{\mathrm{BS}}}{S_{\mathrm{ref}}} + \boldsymbol{f}_{\mathrm{BS}} \tag{2}$$

By using Eq. (2), we can arrange Eq. (1) in the following form:

$$\boldsymbol{f} = \int_{\mathrm{FB}} p_w \boldsymbol{n}\,\mathrm{d}s + \int_{\mathrm{FB}} \tau_w \boldsymbol{t}\,\mathrm{d}s - \frac{2}{\gamma M_\infty^2}\frac{S_{\mathrm{BS}}}{S_{\mathrm{ref}}} + \boldsymbol{f}_{\mathrm{BS}} \tag{3}$$

where in Eq. (3) force on the base of the body is to be obtained by an empirical relation, which will be discussed later.

The surface friction stress in Eq. (3) is defined in terms of a nondimensional local skin-friction coefficient C_f

$$\tau_w = \tfrac{1}{2} C_f \rho_\infty V_\infty^2 \tag{4}$$

Using the force components defined in Eq. (3), drag force can be calculated as follows:

$$D = f_x \cdot \cos\alpha \cdot \cos\beta - f_y \cdot \sin\beta + f_z \cdot \sin\alpha \cdot \cos\beta \tag{5}$$

Calculation of Skin Friction

To obtain the local skin-friction coefficient given in Eq. (3) for high-speed turbulent compressible flows around flat plates at zero angle of attack, van Driest's semianalytical method[6,7] is used. The skin-friction models for laminar[12] and turbulent flows are as follows.

For $Re < 2540$ (laminar),

$$C_f = 0.664\left(1/\sqrt{Re}\right) \tag{6a}$$

and for $Re > 2540$ (turbulent),

$$\frac{0.242}{C_f^{\frac{1}{2}}\{[(\gamma-1)/2]M^2\}^{\frac{1}{2}}}(\sin^{-1}\kappa + \sin^{-1}\sigma) = 0.41 + \log_{10}(Re_x \cdot C_f) - f(n)\log_{10}\left(\frac{T_w}{T_e}\right) \tag{6b}$$

where

$$\kappa = \frac{2A^2 - B}{(B^2 + 4A^2)^{\frac{1}{2}}}, \qquad \sigma = \frac{B}{(B^2 + 4A^2)^{\frac{1}{2}}} \tag{6c}$$

$$A^2 = \frac{[(\gamma-1)/2]M^2}{T_w/T_e}, \qquad B = \frac{1 + [(\gamma-1)/2]M^2}{T_w/T_e} - 1 \tag{6d}$$

In Eq. (6) $f(n)$ is a function of the exponent n in the power viscosity law $\mu = \text{const} \cdot T^n$ and depends on the law assumed for the mixing length l. Thus, when the Prandtl mixing length $l = K \cdot y$ is assumed, where y is the distance from the wall normal to the flow, then $f(n) = \frac{1}{2} + n$; when the von Kármán mixing length $l = K(\mathrm{d}u/\mathrm{d}y)/(\mathrm{d}^2u/\mathrm{d}y^2)$ is assumed, then $f(n) = n$. In the present work, the von Kármán mixing length is assumed, and $f(n) = n = 0.7$ is used.[12] The ratio of wall temperature to boundary-layer edge temperature (T_w/T_e) is obtained from the following recovery factor definition[12]:

$$r = \frac{T_{\mathrm{aw}} - T_e}{T_{0e} - T_e} \approx f(Pr) \tag{7}$$

For high-speed fluid flow, the wall is assumed to be insulated and therefore adiabatic wall temperature may be used for the wall temperature. Thus, by using Eq. (7), we can calculate (T_w/T_e) as follows:

$$T_w/T_e = 1 + r[(\gamma-1)/2]M^2 \tag{8}$$

The value of the recovery factor r varies from 0.85 for laminar flow to 0.88 for turbulent flow.[12] To calculate the local Reynolds number $Re_l = \rho V l/\mu$, values of velocity V and density ρ, as well as the Mach number on the surface of the body, are obtained from the Euler flow solver USER3D. Characteristic length l in the definition of Reynolds number is set to be the distance from the center of the surface mesh to the nose of the body or to the leading edge of the fin. The viscosity μ is calculated by Sutherland's law as follows:

$$\mu/\mu_0 = (T/T_0)^{\frac{3}{2}}[(T_0 + s)/(T + s)] \tag{9}$$

where $\mu_0 = 1.716 \times 10^{-5}$ N·s/m^2, $T_0 = 273$ K, and $s = 111$ K for air.[12]

Equation (6b) is solved iteratively by use of the Newton–Raphson method.

Calculation of Base Drag

Base drag calculations are based on the empirical method as suggested by Refs. 13 and 14. In this method, the axial force acting on the base is obtained by integrating the experimentally obtained base pressure, which is assumed to be uniform throughout the base. Figure 1 gives the base pressure variation as a function of Mach number for a basic body shape with the following limitations: 1) The body is axisymmetric, with zero boattail angle. 2) The fineness ratio is greater than 5. 3) The Reynolds number based on missile length is high enough (10^6–10^8) to ensure a turbulent boundary layer over most of the body length. 4) The body has no fins. These conditions are not as restrictive as they appear. The base pressure is not dependent on the body length when the body is long enough to allow the surface pressure to return to ambient pressure before it reaches

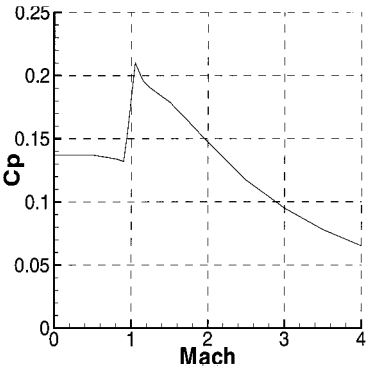

Fig. 1 Variation of the pressure coefficient at the base.[13]

the base. Despite the first and the fourth limitations the method can be applied to finned bodies and bodies with boattail afterbody as suggested in Refs. 14 and 15 provided that proper corrective terms are included in the formulation.

Flow Solver

An unstructured Euler solver, USER3D,[8] is used to calculate the flowfield around the missile configurations. This code, which was previously validated with experimental test results,[9–11] employs a fully conservative, cell-centered, finite volume method applied to the tetrahedral cells of the computational grid. Second-order spatial discretization is based on Roe's flux difference splitting method.[16] An m-stage Runge–Kutta time-stepping scheme[17] is used for time integration. Local time stepping and implicit residual smoothing accelerate convergence to steady state.

Higher-order interpolation and reconstruction schemes together with a total variation diminishing limiter scheme are incorporated into the code to enhance the numerical accuracy of the computations. In this way, higher-order accuracy in space is obtained even in highly stretched grids.

Governing Equations

The time-dependent Euler equations for an ideal compressible fluid in the absence of external forces are given in integral form as

$$\frac{\partial}{\partial t}\iiint_{\Omega} \boldsymbol{Q}\,\mathrm{d}V + \iint_{\partial\Omega} \boldsymbol{F}(\boldsymbol{Q})\cdot\boldsymbol{n}\,\mathrm{d}S = 0 \tag{10}$$

where Ω represents the physical domain with a boundary $\partial\Omega$. The vectors $\boldsymbol{Q}$ and $\boldsymbol{F}$ are given by

$$\boldsymbol{Q} = \begin{Bmatrix} \rho \\ \rho u \\ \rho v \\ \rho w \\ e \end{Bmatrix}, \qquad \boldsymbol{F}(\boldsymbol{Q})\cdot\boldsymbol{n} = (\boldsymbol{V}\cdot\boldsymbol{n}) \begin{Bmatrix} \rho \\ \rho u \\ \rho v \\ \rho w \\ e+p \end{Bmatrix} + p \begin{Bmatrix} 0 \\ n_x \\ n_y \\ n_z \\ 0 \end{Bmatrix} \tag{11}$$

where n_x, n_y, and n_z are the Cartesian components of the exterior surface unit normal $\boldsymbol{n}$ on the boundary $\partial\Omega$. Pressure can be expressed as

$$p = (\gamma - 1)\left[e - \tfrac{1}{2}\rho(u^2 + v^2 + w^2)\right] \tag{12}$$

Boundary Conditions

A flow tangency condition was imposed on the walls and symmetry planes by setting the velocities on the boundary faces to their cell-center values and then subtracting the component normal to the solid surface. Density and pressure boundary conditions were simply set to the cell-centered values.

Characteristic boundary conditions were applied to the far-field boundary for each computation using the fixed and extrapolated Riemann invariants corresponding to the incoming and outgoing waves. The incoming Riemann invariant is determined from the freestream flow, and the outgoing invariant is extrapolated from the interior domain. The invariants are used to determine the locally normal velocity component and speed of sound. At the outflow boundary, the two tangential velocity components and the entropy were extrapolated from the interior, whereas at the inflow boundary, they were specified as having the far-field values. These five quantities provide a complete definition of the flow in the far field.

Grid Generation

The unstructured grids used for the Euler computations were generated using I-DEAS™. Although this tool is not very convenient for generating grids suitable for the present CFD studies, various control features of the code are used until an appropriate grid distribution is achieved. One of the basic advantages of using this tool for grid generation lies in that the geometry comes directly from this design package. Thus, any major modification made to the external geometry of the missile is passed directly to the CFD analysis.

Results and Discussion

Test Case 1: NASA X-1839 Geometry

The details of the geometry used for this test case are given in Ref. 18. It has a 3.5-caliber forebody with an ogive nose followed by a cylindrical body and four straight tail fins with aspect ratio of 0.15. The fineness ratio of the body is 10. Cross sections of fins are of modified-wedge type with a constant thickness ratio of $t/c = 0.0144$ with 10-deg bevelled leading and trailing edges.

The unstructured Euler grid generated for this geometry with 315,286 tetrahedral cells with 58,518 nodes and 18,400 boundary faces for the half-body is given in Fig. 2. All of the Euler computations are performed at zero angle of attack and at Mach numbers ranging from $M = 2$ to 4.

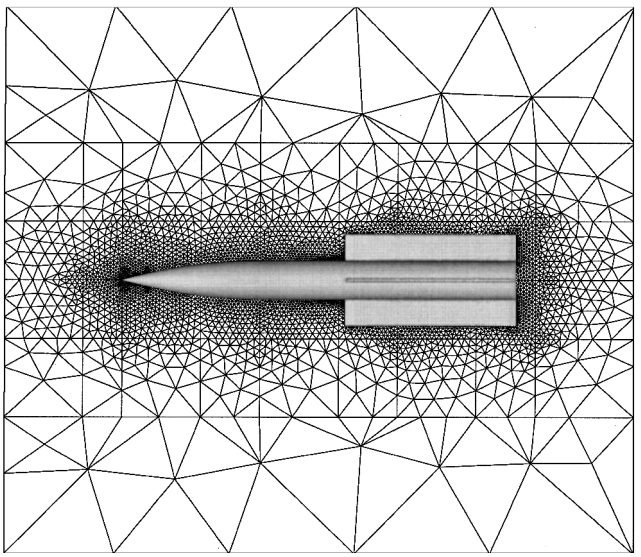

Mesh on the symmetry plane

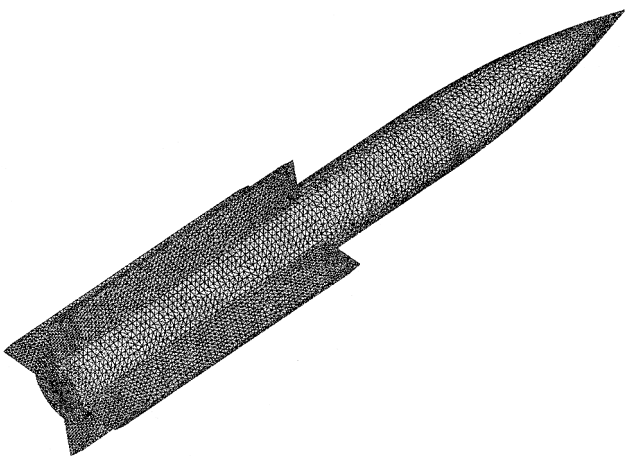

Surface mesh on the geometry

Fig. 2 Mesh for NASA X1839 geometry.

The present approach for predicting the drag coefficient is performed at a freestream Reynolds number per length of 9.84×10^6 m^{-1}. Turbulence is maintained throughout the experiments by boundary-layer trips. Therefore, all calculations are performed using a turbulent skin-friction model. The aim of this test case is to see the effect of Mach number on the results of the present technique. Figure 3 shows the variation of base drag, forebody drag, and total drag coefficients with Mach number M and also compares the computational drag results with the experimental data.[18] Cross-sectional body area is used as the reference area. Observe that the computational total drag results are in good agreement with the experimental values. The computational total drag results overestimate the experimental values for smaller Mach numbers. The accuracy of the results increases with increasing Mach number. The discrepancies observed between the computational and the experimental results at low Mach numbers can be attributed to viscous effects becoming more dominant at low speeds, as discussed in the methodology section.

Test Case 2: ONERA Body–Tail Geometry

The second test case is another conventional missile geometry whose details are given in Refs. 9–11. The nose section of this geometry is a tangent ogive with a 3-caliber forebody followed by a cylindrical body and four straight tail fins with an aspect ratio of 1. The tail fins have a wedge cross section and a constant thickness ratio of $t/c = 0.07$ at the midchord along the span. The leading edges of fins have a sweep angle of 33.69 deg. The fineness ratio of the overall geometry is 16.

Figure 4 shows the unstructured Euler grid generated for this geometry with 297,164 cells with 54,029 nodes and 17,602 boundary faces for the half-body. All of the Euler computations are performed at a freestream Mach number of $M = 2.0$ and at different angles of attack ranging from 1 to 20 deg. Calculations are performed at a freestream Reynolds number per length of 0.7×10^6 m^{-1}. Turbulence is maintained throughout the experiments by boundary-layer trips. Therefore, all calculations are performed using a turbulent skin-friction model. Comparison of experimental and computational C_D values is given in Table 1. Figure 5 presents the variation of drag coefficient C_D with angle of attack α at constant Mach number $M = 2.0$ and also compares the present results with the experimental data. Cross-sectional body area is used as the reference area. The results of the computation are in very good agreement with the experimental results up to 15-deg angle of attack and in fairly good agreement up to 20-deg angle of attack. The increasing deviations with increasing angle of attack are believed to be due to the unsolved viscosity effects, which become more dominant at high angles of

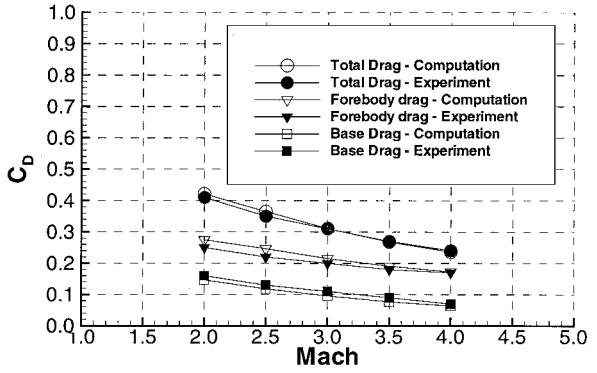

Fig. 3 Variation of total and base drag coefficients for NASA X-1839 geometry.

Table 1 C_D for ONERA body–tail geometry

α, deg	C_D, exp	C_D, computation
1	0.3132	0.3047
5	0.3967	0.3932
10	0.6935	0.6962
15	1.2864	1.3130
20	2.3427	2.5449

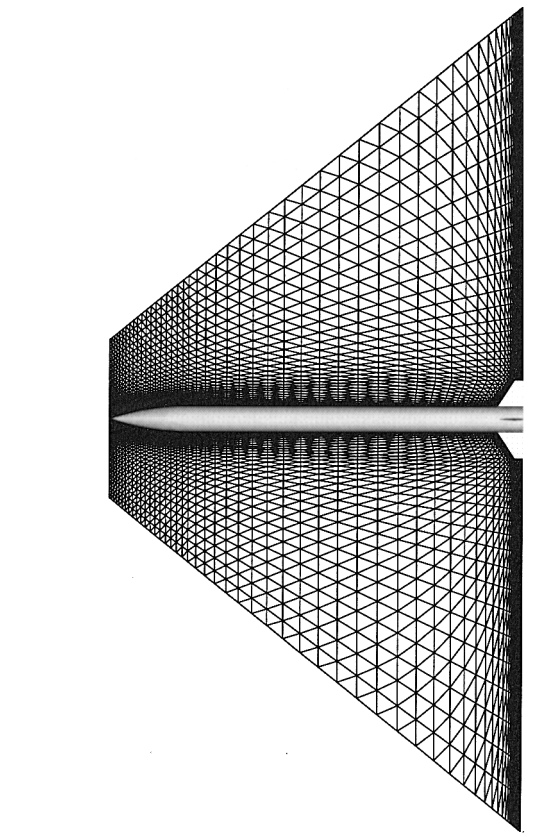

Mesh on the symmetry plane

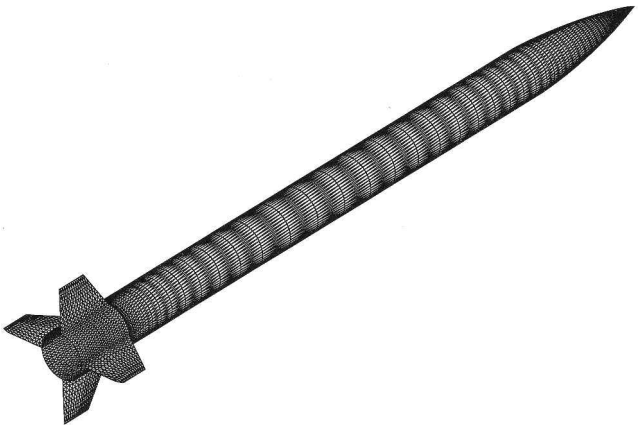

Surface mesh on the geometry

Fig. 4 Mesh for ONERA body–tail geometry.

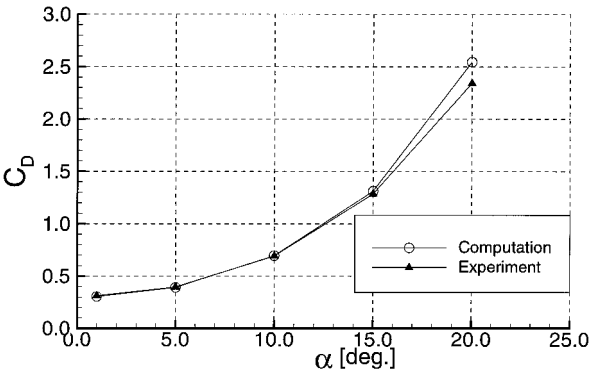

Fig. 5 Variation of the drag coefficient for ONERA body–tail geometry.

attack as discussed in the methodology section. Comparison of the base drag could not be made due to lack of experimental data.

Test Case 3: NASA X-2774 Geometry

The third test case is different from the other two test cases in terms of its 45-deg roll orientation and its boattail-shaped afterbody. The details of this geometry are given in Ref. 19. The body has a fineness ratio of 13.06 and consists of a 3-caliber nose, a cylindrical afterbody, and a 4-deg boattail afterbody. The geometry is provided with four tail fins with aspect ratio of 0.418. Fins have wedge-type cross section and a constant thickness ratio of $t/c = 0.07$ at the midchord along the span.

The unstructured Euler grid generated for this geometry with 225,600 cells with 43,482 nodes and 20,308 boundary faces for the half-body is given in Fig. 6. All of the Euler computations

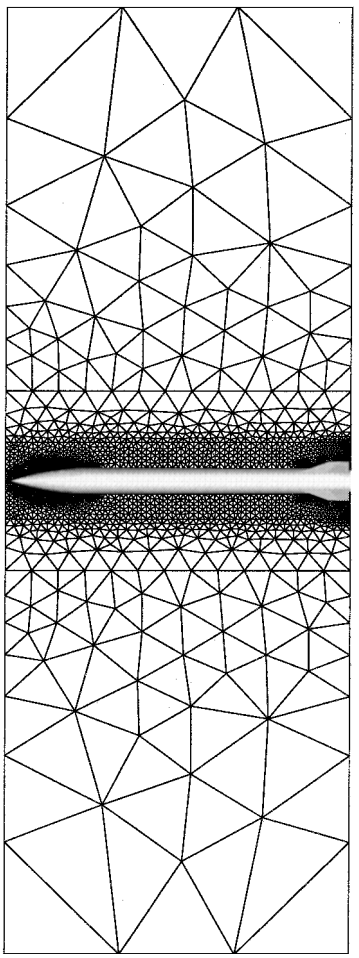

Mesh on the symmetry plane

Surface mesh on the geometry

Fig. 6 Mesh for NASA X-2774 geometry with T9 fins.

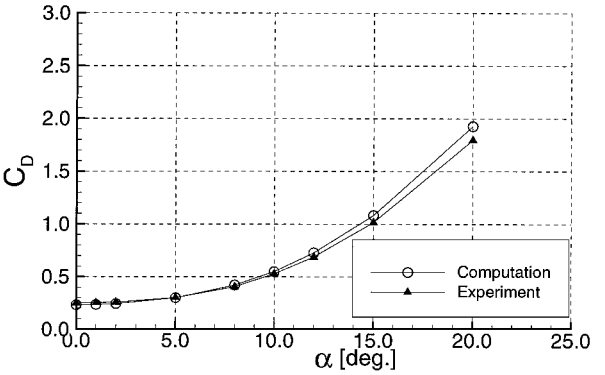

Fig. 7 Variation of the drag coefficient for NASA X-2774 geometry with T9 fins.

are performed at a freestream Mach number of $M = 2.86$ and at different angles of attack ranging from 0 to 20 deg. The calculations are performed at a freestream Reynolds number per length of 8.24×10^6 m^{-1}. Turbulence is maintained throughout the experiments by boundary-layer trips. Therefore, all calculations are performed using a turbulent skin-friction model. The variation of drag coefficient C_D with angle of attack α at constant Mach number $M = 2.86$ is indicated in Fig. 7. The results of the present technique are also compared with those of experiments in Fig. 7. Cross-sectional body area is used as the reference area. It is observed that all of the computational results up to 15-deg angle of attack are in good agreement with the experimental data and are in fairly good agreement up to 20-deg angle of attack, as in the second test case. This similarity indicates that the 45-deg orientation of the tail fins does not have a significant effect on the technique applied. It is also seen that the computational results have not deviated due to the presence of boattail afterbody, although a relatively simple base drag model is used. The solutions are observed to deviate from the experimental data with increasing angle of attack, due to the inherent behavior of Euler solutions at high angles of attack. Comparison of the base drag could not be made due to lack of experimental data.

Conclusions

An approach to predict aerodynamic drag coefficient for missile geometries based on addition of friction drag and base drag on an Euler solution is discussed. Quite accurate results can be obtained with this technique without solving the viscous flow equations.

Compared to a Navier–Stokes solution, very significant reduction in computational time is observed because the method does not involve any differential equations for viscosity terms. Results can be obtained within seconds (less than 1 min even for a fine mesh with a single processor of the SGI ORIGIN 2000 computer) once the Euler solution is available. The drag prediction speed of the present method depends on the speed of the Euler solver used. The unstructured Euler solver, USER3D, used in the current work is a fast upwind solver (prediction of one coefficient takes 15 min in SGI ORIGIN-2000 parallel computer with 8 processors for 200,000 cells). This technique with a powerful CAD and grid generation tool will speed up the preliminary design phase of a missile a considerable amount.

The three test cases used for the validation of the present approach to predict drag coefficient at supersonic speeds give quite promising results. The test cases are chosen so that the effects of different geometrical considerations, Mach number, and angle of attack can be observed on the results of the present technique. It is observed that the present method can be applied to different geometries at various flight conditions.

As an overall evaluation, it can be said that the current approach seems to be quite successful in predicting the drag coefficient for conventional missile geometries at supersonic speeds and at low to moderate angles of attack. The accuracy of the results and the high speed of the computations are the factors that make the technique a very attractive and a reliable tool that can be used during the preliminary design phases.

Acknowledgments

The authors thank E. Tarhan and U. Kakaşçı from the Engineering Development Department of ROKETSAN Missiles Industries, Inc., for their help on this study. The valuable advice of N. Alemdaroğlu about the present work is also appreciated.

References

[1]Burns, K. J., Deters, K. J., Stoy, S. L., Vukelich, S. L., and Balke, W. B., "Missile DATCOM User's Manual—Revision 6/93," Wright Lab., WL-TR-93-3043, Wright–Patterson AFB, OH, June 1993.

[2]Genty, A. E., Smyth, D. N., and Oliver, W. R., "The Mark IV Supersonic-Hypersonic Arbitrary-Body Program," Douglas Aircraft Co., AD-778 444, Long Beach, CA, Nov. 1973.

[3]Sloof, J. W., "Technical Status Review on Drag Prediction and Analysis from Computational Fluid Dynamics: State of the Art," Advisory Rept. 256, AGARD, June 1989.

[4]van Dam, J. P., Nikfetrat, K., Chang, I. C., and Vijgen, P. M. H. W., "Drag Calculations of Wings Using Euler Methods," AIAA Paper 91-0338, Jan. 1991.

[5]van Dam, J. P., Nikfetrat, K., Wong, K., and Vijgen, P. M. H. W., "Drag Prediction at Subsonic and Transonic Speeds Using Euler Methods," *Journal of Aircraft*, Vol. 32, No. 4, 1995, pp. 839–845.

[6]van Driest, E. R., "Turbulent Boundary Layer in Compressible Fluids," *Journal of the Aeronautical Sciences*, Vol. 18, No. 3, 1951, pp. 145–160.

[7]van Driest, E. R., "The Problem of Aerodynamic Heating," *Aeronautical Engineering Review*, Vol. 15, Oct. 1956, pp. 26–41.

[8]Oktay, E., "USER3D, 3-Dimensional Unstructured Euler Solver," ROKETSAN Missile Industries, Inc., SA-RS-RP-R 009/442, Ankara, Turkey, May 1994.

[9]Oktay, E., Alemdaroğlu, N., Tarhan, E., Champigny, P., and d'Espiney, P., "Unstructured 3D-Euler Computations for Missile at Supersonic Speeds and High Angles of Attack," AIAA Paper 98-0392, Jan. 1998.

[10]Oktay, E., Alemdaroğlu, N., Tarhan, E., Champigny, P., and d'Espiney, P., "3D Euler and Thin Layer Navier–Stokes Solutions for Missiles at Supersonic Speeds and High Angles of Attack," *Research and Technology Organization (RTO) Meeting Proceedings 5 on Missile Aerodynamics*, 1998, pp. 27.1–27.12.

[11]Oktay, E., Alemdaroğlu, N., Tarhan, E., Champigny, P., and d'Espiney, P., "Euler and Navier–Stokes Solutions for Missiles at High Angles of Attack," *Journal of Spacecraft and Rockets*, Vol. 36, No. 6, 1999, pp. 850–858.

[12]White, F. M., *Viscous Fluid Flow*, 2nd ed., McGraw–Hill, New York, 1974, pp. 29, 556.

[13]Stoney, E. W., Jr., "Collection of Zero-Lift Drag Data on Bodies of Revolution from Free-Flight Investigations," NASA TR R-100, July 1961.

[14]"Handbook of Supersonic Aerodynamics," Bureau of Naval Weapons, NAVWEPS Rept. 1488, Vol. 3, Washington, DC, 1961, pp. 279–293.

[15]Mason, A. L., Devan, L., Moore, F. G., and McMillan, D., "Aerodynamic Design Manual for Tactical Weapons," U.S. Naval Surface Weapons Center, NSWC/TR 81-156, Dahlgren, VA, July 1981.

[16]Roe, P. L., "Characteristic-Based Schemes for the Euler Equations," *Annual Review of Fluid Mechanics*, Vol. 18, 1986, pp. 337–365.

[17]Jameson, A., and Baker, T. J., "Solution of the Euler Equations by Finite Volume Methods Using Runge–Kutta Time Stepping Schemes," AIAA Paper 81-1259, June 1981.

[18]Spearman, M. L., and Trescot, D. C., Jr., "Effects of Wing Planform on the Static Aerodynamics of a Cruciform Wing Body Missile for Mach Numbers up to 4.63," NASA TM X-1839, July 1969.

[19]Trescot, D. C., Jr., Foster, G. V., and Babb, C. D., "Effect of Fin Planform on the Aerodynamic Characteristics of Wingless Missile with Aft Cruciform Controls at Mach 1.60, 2.36, and 2.86," NASA TM X-2774, July 1973.

J. R. Maus
Associate Editor